

Semiconductor nanowire lasers

Samuel W. Eaton^{1*}, Anthony Fu^{1,2*}, Andrew B. Wong^{1,2}, Cun-Zheng Ning^{3,4}
and Peidong Yang^{1,2,5,6}

Abstract | The discovery and continued development of the laser has revolutionized both science and industry. The advent of miniaturized, semiconductor lasers has made this technology an integral part of everyday life. Exciting research continues with a new focus on nanowire lasers because of their great potential in the field of optoelectronics. In this Review, we explore the latest advancements in the development of nanowire lasers and offer our perspective on future improvements and trends. We discuss fundamental material considerations and the latest, most effective materials for nanowire lasers. A discussion of novel cavity designs and amplification methods is followed by some of the latest work on surface plasmon polariton nanowire lasers. Finally, exciting new reports of electrically pumped nanowire lasers with the potential for integrated optoelectronic applications are described.

In 1916, Albert Einstein theorized the existence of stimulated emission, thus providing the underpinnings of lasing action¹. Expanding on these principles, Charles Townes and Arthur Schawlow laid the foundation² for Theodore Maiman to demonstrate the first working laser using a ruby gain medium³. Since these early developments, the use of lasers has been extended to many areas, and lasers have evolved considerably owing to innovations in the fields of materials, optics and electronics (FIG. 1). The addition of new functionalities and improved properties has led to the emergence of new industries and contributed to the growth of existing industries⁴.

From the time of its inception to the present day, there has been intense interest in the miniaturization of the laser. The advent of compact semiconductor lasers has fundamentally changed the pace and nature of miniaturization and enabled the development of new technologies, such as optical fibre communications, image scanning, compact disc players, barcode scanners, laser printers, and compact light detection and ranging (LIDAR) systems⁵. Recently, the push to shrink lasers has provided new types of devices, such as vertical-cavity surface-emitting lasers⁶, microdisc lasers⁷ and photonic crystal lasers⁸, some of which are used commercially. Although miniaturization has allowed the widespread adoption of lasers, the next frontier in laser research is set to revolutionize the field of optoelectronics. In the past decade, academic research has increasingly focused on exploring and developing nanoscale lasers for applications in on-chip photonic devices⁹ and ultrasensitive sensors¹⁰. One of the principal areas of research in this field is the semiconductor nanowire: a quasi-one-dimensional semiconductor that simultaneously acts as an optical gain medium and optical cavity

that, in some cases, possesses the intrinsic capability to lase^{9,11,12}. This property, along with the ability to tune the emission wavelength and its potential for electrical integration, makes the nanowire laser a promising candidate for use in the next generation of optoelectronic devices. In this Review, we introduce the concept of the nanowire laser, relate fundamental discoveries of the field to important, recent advances, and offer our perspective on future research directions.

Nanowire laser fundamentals

The first semiconductor nanowires were grown from silicon using a vapour–liquid–solid growth mechanism that used a gold metal catalyst to facilitate 1D, crystalline growth¹³. Using this vapour–liquid–solid approach, dense arrays of ZnO nanowires were grown, for which the first observation of laser action was reported¹⁴; therefore, this work introduced a new and facile approach for the fabrication of nanoscale lasers (FIG. 2). In contrast to traditional ‘top-down’ fabrication techniques that etch macroscopic crystals to define nanoscale features, these nanowire structures were grown from the ‘bottom up’ on sapphire substrates coated with gold by simply heating a mixture of ZnO and graphite in an argon atmosphere¹⁵. The natural anisotropy and the associated facets of the wurtzite structure of ZnO resulted in the formation of the nanowire optical cavity.

Although this demonstration represented a breakthrough in the miniaturization of the semiconductor laser, several questions remained regarding the nature of the optical cavity. It was postulated that the nanowire acts as a Fabry–Pérot cavity; however, there was limited experimental evidence to support this claim. The first

¹Department of Chemistry, University of California, Berkeley, California 94720, USA.

²Materials Sciences Division, Lawrence Berkeley National Laboratory, Berkeley, California 94720, USA.

³School of Electrical, Computer and Energy Engineering, Arizona State University, Tempe, Arizona 85287, USA.

⁴Department of Electronic Engineering, Tsinghua University, Beijing 100084, China.

⁵Kavli Energy NanoSciences Institute, Berkeley, California 94720, USA.

⁶Department of Materials Science and Engineering, University of California, Berkeley, California 94720, USA.

*These authors contributed equally to this work. Correspondence to P.Y. p_yang@berkeley.edu

Article number: 16028
doi:10.1038/natrevmats.2016.28
Published online 4 May 2016

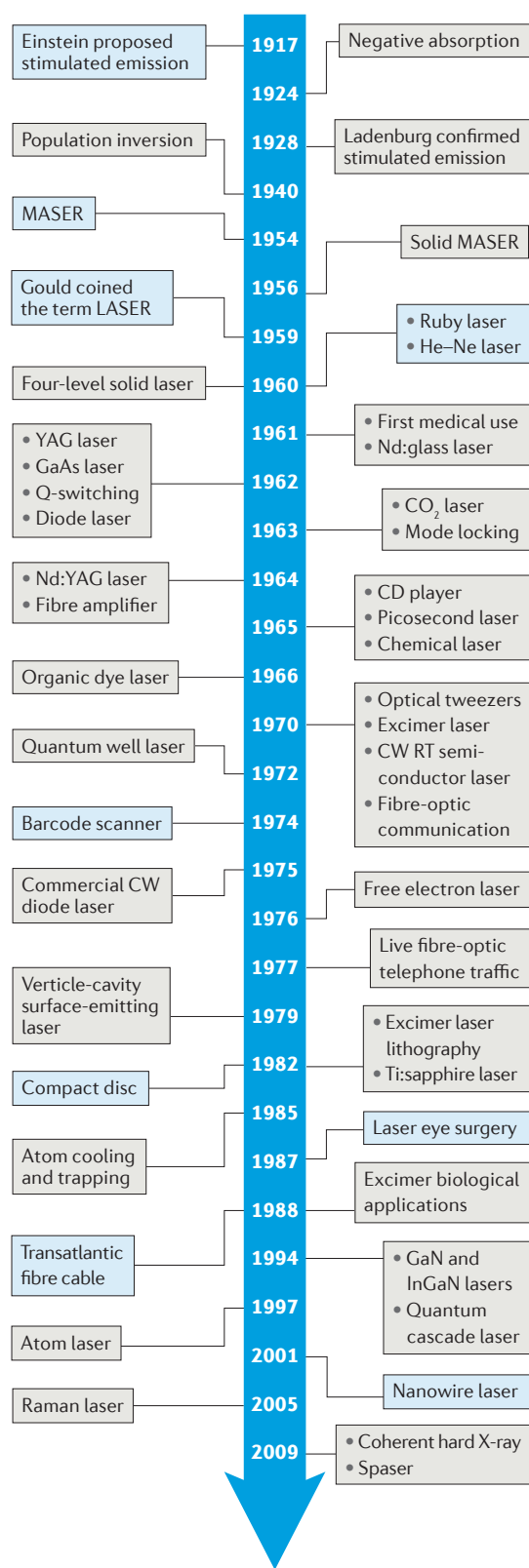


Figure 1 | A brief timeline of laser discovery and development. The advances shown in blue boxes are considered to be some of the most important and have resulted in widespread application or further advances. CW, continuous wave; RT, room temperature; YAG, yttrium aluminium garnet.

reported experiments¹⁴ were performed on an ensemble of nanowires with diameters varying between 20 and 150 nm and lengths between 2 and 10 μm; the resulting spectrum was an average of the signals from many individual nanowires. To further understand the properties of the cavity, single nanowires were obtained by sonication of a nanowire array grown on a sapphire substrate in ethanol followed by drop casting the solution on a new substrate. Near-field scanning optical microscopy was used to examine the spatially resolved photoluminescence of these nanowires when they were excited above the lasing threshold^{16,17}. The emission spectra acquired from the end facets of the nanowires displayed lasing peaks, and spectra from the end facets were much stronger than from the side facets. These results indicated that nanowire lasers were operating by relying on waveguided emission to improve optical feedback in the cavity. This was further supported by reports of a diameter threshold for the lasing process; nanowires below a certain diameter were unable to lase because of insufficient waveguide confinement¹⁸. In addition, the lasing peak spacing could be predicated by assuming a linear relationship between the spacing and the reciprocal of the nanowire length, which is characteristic behaviour for a Fabry–Pérot cavity¹⁹.

Before the discovery of lasing in nanowire arrays, it was unclear if cavities with such small end facets could support lasing, because it was thought that they might induce substantial scattering losses and render the cavity too inefficient to reach the lasing threshold⁹. Amplification in a nanowire Fabry–Pérot cavity relies on the optical feedback from light reflected from the crystalline end facets of the nanowire and propagated back through the gain medium. Lasing is achieved when the round-trip gain exceeds the round-trip losses^{20,21},

$$\Gamma g > \alpha_m + \alpha_p = \frac{1}{2L} \ln \left(\frac{1}{R_1 R_2} \right) + \alpha_p \quad (1)$$

where Γ is the confinement factor, g is the material gain, α_m is the mirror loss, α_p is the propagation loss, L is the cavity length, and R_1 and R_2 are the effective reflection coefficients for each end facet, which are nominally equal. As shown on the right side of equation (1), end facet reflection efficiency has a large role in determining mirror loss and the amount of gain required to reach the lasing threshold. When the nanowires have diameters that are on the same order of magnitude as the wavelength of light, the typical reflection process at the semiconductor/air interface becomes a scattering process. It has been shown theoretically that this ‘effective reflection’ due to scattering at the end of a nanowire can be very different from the reflection magnitude predicted using the standard Fresnel formulae. As the scattering process can, in some cases, significantly increase the effective reflection of the end facets, mirror loss may be reduced²².

Another uncertainty encountered during the development of nanowire lasers was that it was unclear how much round-trip gain could be produced to compensate for mirror loss, because nanowires are orders of magnitude shorter in length than conventional semiconductor laser cavities. A possible answer was found

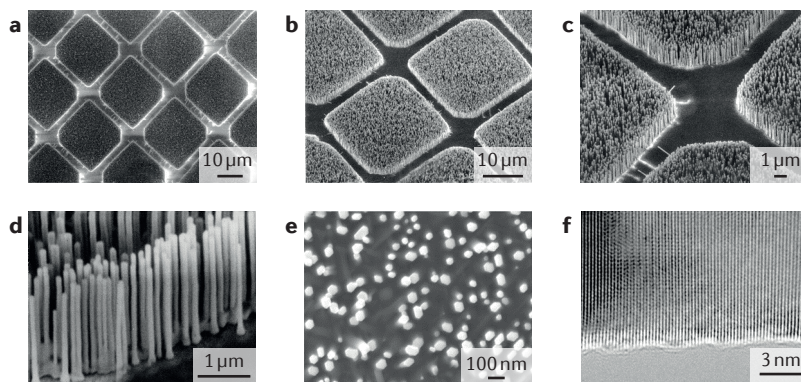


Figure 2 | ZnO nanowire arrays formed the first nanowire laser cavities. **a–e** | Scanning electron microscopy images of ZnO nanowire arrays grown on sapphire substrates. **f** | High-resolution transmission electron microscopy image of a single-crystalline ZnO nanowire showing no extended defects. Figure is adapted with permission from REF. 14, American Association for the Advancement of Science.

in the confinement factor, which is typically defined as the ratio of the optical energy inside the gain medium to that in the total guided mode^{23,24}. It has been suggested theoretically that the confinement factor in a nanowire laser could be larger than unity²³. This property has been related to the strongly waveguiding nature of the nanowire, in which the actual length of wave propagation may exceed the axial length of the nanowire²⁴. A larger-than-unity confinement factor suggests that modal gain (that is, amplification specific to a given mode), in addition to material gain, may have a role in allowing a nanowire laser to reach the lasing threshold. In practice, this may aid nanowire lasers in achieving lasing, which would not be possible for a different cavity geometry.

As the study of single-nanowire lasers matures, it becomes increasingly important to rigorously model the nanoscale laser. Modelling helps define the lasing threshold, which can be thought of as the amount of excitation necessary to turn the laser ‘on’. Specifically, modelling the transition from amplified spontaneous emission (ASE) to lasing oscillation enables a closer examination of the threshold behaviour. When lasers shrink in mode volume, the definition of the lasing threshold becomes less clear²⁵. This threshold is generally determined from a power plot describing the relationship between the input excitation and the output emission. For a nanoscale laser, the lasing threshold is less distinguished because a larger fraction of the spontaneous emission is coupled into the laser mode. Rate equation analysis to model this relationship helps to define the threshold of nanowire lasers. The coupled rate equations to describe the carrier density and photon density for a single mode in a semiconductor cavity can be defined as

$$\frac{dN}{dt} = \eta P - \frac{N}{\tau_r} - \frac{N}{\tau_{nr}} - \Gamma v_g \alpha (N - N_0) S \quad (2)$$

$$\frac{dS}{dt} = \beta \frac{N}{\tau_r} + \Gamma v_g \alpha (N - N_0) S - \frac{1}{\tau_s} S \quad (3)$$

where N is the carrier density, S is the photon density, P is the pump intensity, η is the pumping efficiency, τ_r and τ_{nr} are the spontaneous emission and non-radiative

lifetime, respectively, τ_s is the photon lifetime, β is the spontaneous emission factor, N_0 is the transparency carrier density, α is the differential gain, Γ is the confinement factor and v_g is the group velocity. The gain is approximated in the linear regime by equation (4):

$$g = \alpha(N - N_0) \quad (4)$$

By solving for these coupled rate equations under steady-state conditions, the photon density can be plotted as a function of pump intensity, as shown in FIG. 3 for various values of β . In this example, the numerical values for α , τ_s , τ_r and τ_{nr} , Γ and N_0 used to construct this plot are obtained from modelling GaN nanowire lasers²⁶. The value of β is the fraction of spontaneous emission coupled into the laser mode of interest. A high β value is crucial for applications, because it improves the nanowire laser emission efficiency and is also necessary for nanowire lasers with high modulation frequency²⁷. In general, as the cavity volume shrinks, the spontaneous emission factor increases and the threshold ‘softens’, making the transition to lasing less abrupt^{25,28}. By fitting the experimental power plot to a calculated plot, the lasing threshold can be more quantitatively defined. Furthermore, by plotting the output power against the pumping power on a log–log scale, the change of the slope of the ‘S’ curve demonstrates a lasing threshold transition that is often associated with the ‘superlinear’ regime^{20,21,29}. Notably, when $\beta = 1$ and τ_{nr} is large compared with τ_r , the S curve becomes a straight line and lasing is seemingly ‘thresholdless’ (FIG. 3; black trace). A recent quantum statistics study of nanoscale lasers suggested that, even without a distinct threshold in the input versus output plot, it may be possible to determine a finite threshold²⁷. Qualitatively, the slope of the S curve may also help to identify false positives in experiments, which may be caused by the nonlinear sensitivity of the detector, insufficient data or the exclusive observation of ASE. In general, quantification of the lasing threshold is always preferable. It should also be noted that β values may be overestimated in the fit depending on the experimental conditions. For example, in the case of a nanowire lying flat on a substrate, a significant fraction of the emission will not be collected during the experiment. This is because lasing emission is more anisotropic than spontaneous emission; therefore, the collection scheme may lead to a slight overestimation of the value of β .

Semiconductors for nanowire lasers

Since its first demonstration, the bottom-up synthesis of semiconductor nanowires with high optical quality has generated tremendous interest in the nanomaterials community because of the potential advantages it offers for the fabrication of nanolasers compared with more conventional top-down techniques. For example, top-down techniques tend to require time-consuming and complex steps, which can result in elevated costs. In addition, extensive fabrication expertise and great care are necessary to produce the high-quality, nanoscale structures required for successful lasing. By contrast, chemical synthesis of nanostructures can be relatively simple and less time consuming. For example, in the case of ZnO nanowires, the synthesis can take just 5–30 minutes

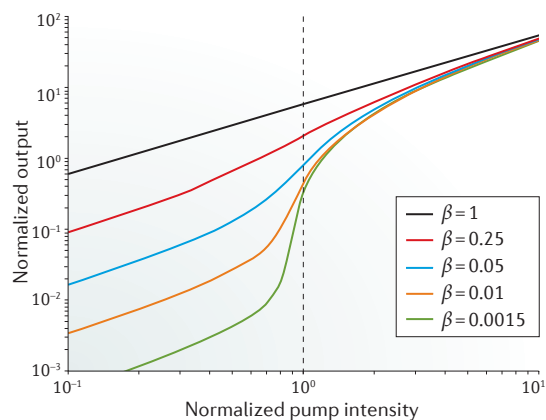


Figure 3 | Calculated power plot of a hypothetical GaN laser with different values of β . The pump intensity is normalized to the lasing threshold. Although clear ‘S’ curve behaviour is demonstrated at low values of β , the transition to ‘thresholdless’ is evident as the value of β increases. β , spontaneous emission factor.

after preparation¹⁵. Another advantage, which has been explored extensively, is that bottom-up techniques can be used to prepare new semiconductor materials suitable for nanowire lasers. This is particularly important because traditional semiconductors, such as ZnO and CdS, are often difficult to handle using conventional cleanroom techniques. The use of relatively simple tube furnaces to grow nanowires of high crystalline quality is attractive for the initial exploration of new materials. These tube furnaces eliminate the need for the sophisticated reactors used in metalorganic chemical vapour deposition or molecular beam epitaxy.

The development of nanowire lasers made from GaN also represents the first extension of the single-nanowire laser to new material systems beyond ZnO. Single-crystalline GaN nanowires were grown in a bottom-up synthesis method for single-nanowire lasers³⁰. One year later, the first example of lasing from a core-shell heterostructure that consisted of a GaN core with an epitaxial shell of $\text{Al}_{0.75}\text{Ga}_{0.25}\text{N}$ was demonstrated³¹. The core-shell nanowires were synthesized by a one-step chemical vapour deposition process with spontaneous phase separation in the synthesized nanowires forming a 5- to 40-nm-thick GaN core. The $\text{Al}_{0.75}\text{Ga}_{0.25}\text{N}$ shell forms a type I junction with GaN and possesses a smaller refractive index than that of GaN (2.54 and 2.25, respectively), which enables this structure to function as a thin GaN nanowire core embedded in AlGaN cladding. These works led to the study of new material systems and heterostructures for nanowire lasers, which are described in the remainder of this Review. Since these early studies, the library of nanowire laser materials has expanded enormously, resulting in nanolasers that emit in the ultraviolet (UV), visible and near-infrared regions. This wide range in emission wavelengths can be seen in demonstrations for ZnO (REFS 14, 17, 30), GaN (REFS 16, 26, 32, 33), InGaN (REF. 34), CdS (REF. 35), CdSe (REF. 36), CdSSe (REF. 37), GaAs (REF. 38), InGaAs (REF. 39), AlGaAs (REF. 40), ZnS (REF. 41), CdSe (REF. 36), GaSb (REF. 42) and InP (REFS 43, 44).

Wavelength selection in nanowire lasers

Many photonics applications could be enabled or enhanced by the use of wavelength-tunable, nanoscale lasers. These applications include sensing⁴⁵, white light generation^{46,47} and optoelectronic integrated circuits¹². Discrete colour tunability can be achieved by using different gain materials, with the ultimate goal of achieving continuous wavelength tunability to tailor emission to a specific application. Another approach to tune the wavelength is by modifying the dielectric environment of the cavity via the excitation intensity³⁰, cavity length⁴⁸, substrate properties⁴⁹ or cavity design^{50,51}. However, this strategy can only be applied for a limited wavelength range and can be impractical to implement in some cases. Here, we focus our discussion on tuning the composition of the gain medium for controlling the emission wavelength.

Alloying is a well-known technique for modifying the bandgap of a material and has been applied to various semiconductors⁵². In alloyed thin films of some materials, issues relating to phase separation due to lattice mismatch have arisen. Many of these problems have been overcome by using nanowires formed under carefully controlled growth conditions. Compositional tunability in $\text{CdS}_x\text{Se}_{1-x}$ nanowires on the same chip was demonstrated³⁷. Through careful control of the temperature gradient in the growth furnace, $\text{CdS}_x\text{Se}_{1-x}$ nanowire arrays were grown with $x=0$ to 1 over a relatively short (1.2-cm-long) substrate. These nanowire arrays exhibited chip position-dependent emission ranging from 498 to 692 nm depending on the composition. Upon optical excitation above the lasing threshold, the nanowires were found to lase across an unprecedented 189-nm-wide wavelength range.

Extending this technique further, the growth of compositionally variable nanoribbons of $\text{CdS}_x\text{Se}_{1-x}$ and $\text{Zn}_y\text{Cd}_{1-y}\text{S}$ was also demonstrated⁵³. These nanoribbons were found to lase from the UV (340 nm) to the near-infrared (710 nm) regions with well-defined growth parameters that provide precise control over the emission wavelength to achieve overlapping coverage across the spectrum. Besides these proven nanowire lasers, other strategies have been developed to grow promising, compositionally graded nanowires. For example, in addition to control of the temperature gradient, a composition gradient in the source material was also exploited to grow $\text{In}_x\text{Ga}_{1-x}\text{N}$ alloy nanowires⁵⁴, whereby the full composition range between InN and GaN was realized for the first time. The demonstrations of alloy composition control through a temperature gradient³⁷ and elemental gradient⁵⁴ led to the simultaneous exploration of both gradients using a growth apparatus that allowed substrate tilting and optimization of the temperature profile^{55,56}. This dual-gradient method enabled the growth of $\text{Zn}_x\text{Cd}_{1-x}\text{S}_y\text{Se}_{1-y}$ in its full composition range from ZnS to CdSe on a single substrate with emission spanning the full visible spectrum⁵⁶. With further development, these methods for synthesizing broadly tunable materials may provide more facile access to high-quality nanowires for lasing.

This concept of compositional control providing emission tunability has also been demonstrated in compositionally graded single nanowires of $\text{CdS}_x\text{Se}_{1-x}$ (REF. 57).

Owing to asymmetric light propagation, a compositionally graded nanowire will only lase at the lowest energy wavelength, because all higher-energy emission is attenuated by the low-bandgap regions of the nanowire⁵⁸. However, by folding the wide-bandgap side of the flexible nanowires into a loop cavity, simultaneous lasing could be observed at different wavelengths in the same nanowire⁵⁹. Tunability over the red-to-green part of the spectrum was achieved through variable optical pumping, such that the output ratio from the two colours could be tuned continuously between the two colours. By incorporating a third, blue loop cavity, this approach may allow for continuous tunability across the entire visible spectrum. The most recent strategy for controlling the lasing wavelength of compositionally graded CdS_xSe_{1-x} nanowires relies on cleaving the nanowires to the required size⁶⁰ (FIG. 4a). The lasing wavelength may be selected by using a bend-to-fracture method on the nanowire to remove undesired low-bandgap material. The free spectral range — or the mode spacing dictated by the length of the Fabry–Pérot cavity — may be tuned by removing material from the high-bandgap end without significantly changing the lasing wavelength. These two operations can provide highly tunable, single-mode nanowire lasers. This approach was demonstrated to yield nanowire lasers operating over a wide spectral range (119 nm).

Recently, methyl ammonium lead halide perovskites were identified as a promising gain material for application in various optoelectronic systems^{61,62}. These inorganic–organic hybrid materials exhibit high absorption cross sections, efficient photoluminescence, long diffusion lengths and low trap-state densities⁶¹. Initial reports of ASE in hybrid perovskite thin films indicated that methyl ammonium lead iodide (MAPbI₃) has high material gain with a low ASE threshold⁶³. In addition, by using a mixture of methyl ammonium salts for film fabrication, wide wavelength tunability of the ASE peak was demonstrated. This study was shortly followed by detailed photophysical studies⁶⁴, in which a bimolecular free carrier electron–hole recombination mechanism was reported to be responsible for the 70% photoluminescence quantum efficiency observed in thin films of MAPbI₃. In addition to ASE from thin films, low-threshold lasing in MAPbI₃ films contained in a vertical-cavity optical structure was also demonstrated⁶⁵. These initial reports established the ease with which perovskite materials could be made to lase while also providing the foundation for other laser cavity designs.

Recently, lasing in a perovskite nanowire cavity was reported for the first time, with the crucial breakthrough being the synthesis of nanowires with high optical quality and suitable dimensions⁶⁶. The perovskite nanowires were grown by exposing a lead acetate film to a solution of methyl ammonium halide salt, and the resulting nanowires were shown to lase at room temperature under optical excitation. Furthermore, the ability to tune the composition of the nanowires by changing the ratio of the halide salts in the growth solution enabled lasing across the visible spectrum (FIG. 4b). Although these nanowires possess remarkable optical properties, it is even more

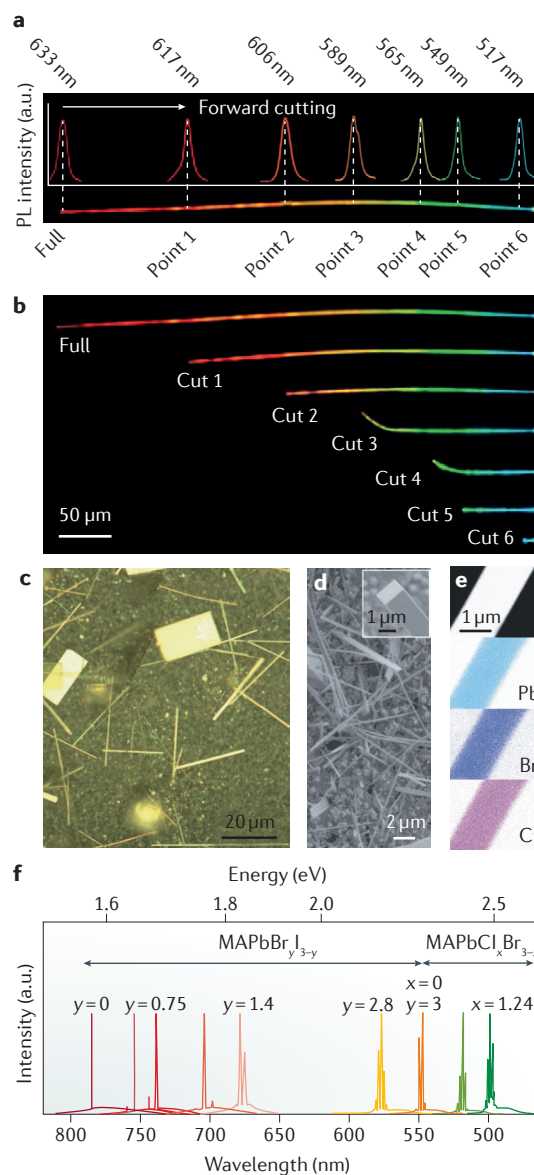


Figure 4 | Nanowire lasers offer broad wavelength selection. **a,b** | Compositionally graded CdS_xSe_{1-x} nanowire photoluminescence spectra and optical images under laser excitation demonstrating nanowire position-dependent emission. **c,d** | Optical and scanning electron microscopy (SEM) images of alloyed methyl ammonium lead halide nanowires and plates. **e** | SEM image (top) and energy dispersive X-ray spectroscopy images depicting the elemental distribution of Pb, Br and Cl in the alloyed nanowire. **f** | Broad wavelength tunability achieved over nearly 300 nm by tuning the elemental composition of the nanowire laser. a.u., arbitrary units; PL, photoluminescence. Panels **a** and **b** are adapted with permission from REF. 60, American Chemical Society. Panels **c–f** are from REF. 66, Nature Publishing Group.

impressive that they were grown under ambient conditions. This is in stark contrast to the synthesis methods used to produce most other nanowire lasers, which rely on high temperatures or vacuum synthesis processes. Another notable approach involved the growth and

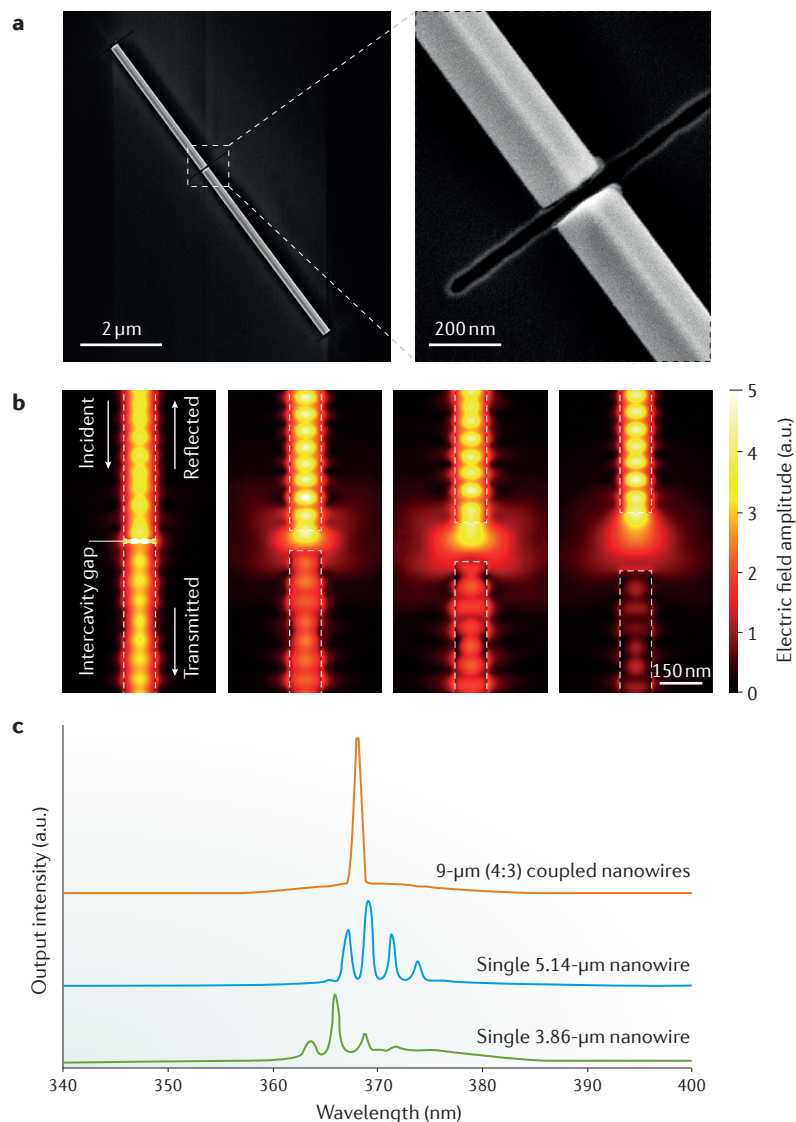


Figure 5 | Creating a cleaved-coupled cavity nanowire laser. a | Scanning electron micrographs of a GaN cleave-coupled nanowire laser cavity. The gap size and position were chosen to optimize the cavity for single-mode lasing. **b** | Finite-element method simulations showing the transmission and reflectance of a waveguide mode for different gap sizes. **c** | Photoluminescence spectra for the lasing modes of the individual nanowire components (green and blue) and the coupled nanowires (red). a.u., arbitrary units. Figure is adapted with permission from REF. 26, National Academy of Sciences.

subsequent exposure of PbI_2 nanowires to methyl ammonium halide vapour to produce perovskite nanowires⁶⁷. Although the nanowire morphology was maintained, the lasing properties were significantly less impressive than those achieved with the solution-phase growth method that produced superior-quality nanowire lasers.

Although they exhibit excellent performance, hybrid perovskite nanowires are well known for their intrinsic instability^{68,69}. Various strategies have been pursued to improve their stability, with many focused on replacing the reactive methyl ammonium cation with an alternative cation. A recent report demonstrated that formamidinium ($\text{CH}(\text{NH}_2)_2^+$) lead halide nanowires offer considerably improved stability compared with methyl ammonium

lead halide nanowire lasers, and they successfully lase for over 10^8 excitation cycles while still offering a high degree of wavelength tunability⁷⁰. Alternatively, the organic cation can be abandoned altogether, because cation replacement with caesium has opened up a new route to highly luminescent, stable materials⁷¹. The first reports of colloidal nanocrystals made from caesium lead halides demonstrated similar wavelength tunability to that of the hybrid perovskite materials and remarkably high photoluminescence quantum efficiencies^{72,73}. Moreover, ASE was demonstrated in thin films of nanocrystals with a low lasing threshold compared with that of perovskite materials^{74,75}. These reports were shortly followed by the synthesis and characterization of colloidal⁷⁶ and non-colloidal⁷⁷ caesium lead halide perovskite nanowires. The non-colloidal nanowires were found to have comparable lasing thresholds and Q-factors to those of hybrid perovskite nanowire lasers, albeit with one significant difference: the all-inorganic perovskite nanowires were found to be ultrastable under lasing conditions, continuing to lase even after 10^9 excitation cycles⁷⁷. High stability under ambient conditions was also observed during both lasing and storage. Mild growth conditions, excellent performance and constantly increasing stability make perovskite-based nanowire lasers a promising material for the future.

New nanowire laser cavity structures

The compact form factor of 1D nanowire lasers has also enabled the development of nanowires for photonic applications, such as nanoscale optical routing⁷⁸, nanoscale electro-optic modulators⁷⁹ and single-cell probes⁸⁰. A range of alternative cavity structures has also been explored through either bottom-up or top-down fabrication strategies. One of the first alternative structures was an adaptation of the vertical ZnO array; by carefully controlling the nanowire growth conditions⁸¹, dendritic ZnO nanowires could be grown from a ZnO backbone⁸². The ZnO nanowires in these linear, regularly spaced arrays exhibited ASE at elevated pumping thresholds, which was similar to the previously reported planar arrays, and were hypothesized to form modified Fabry–Pérot cavities with only a single, well-defined end facet.

The physical manipulation of flexible nanowires provides a method for generating cavities of arbitrary geometry with improved performance. One example is the ring-resonator nanowire laser. Ring resonators are typically formed by bending a pre-existing nanowire into a continuous loop. If the overlapping nanowire sections are sufficiently coupled to allow for recirculation of light around the loop, optical feedback is increased in the system, thereby lowering the lasing threshold. The first example of a nanowire ring resonator was made from GaN, which was manipulated into a loop with the two ends side by side⁵⁰. Cavity modes were observed in the spontaneous emission and lasing spectra, indicating the formation of a circular resonator. In this case, when the nanowire ring-resonator cavities were decoupled into linear cavities, the Q-factor of the resonator dropped by 40% (that is, the ring resonators have larger Q-factors than those of their linear counterparts). The ring-resonator

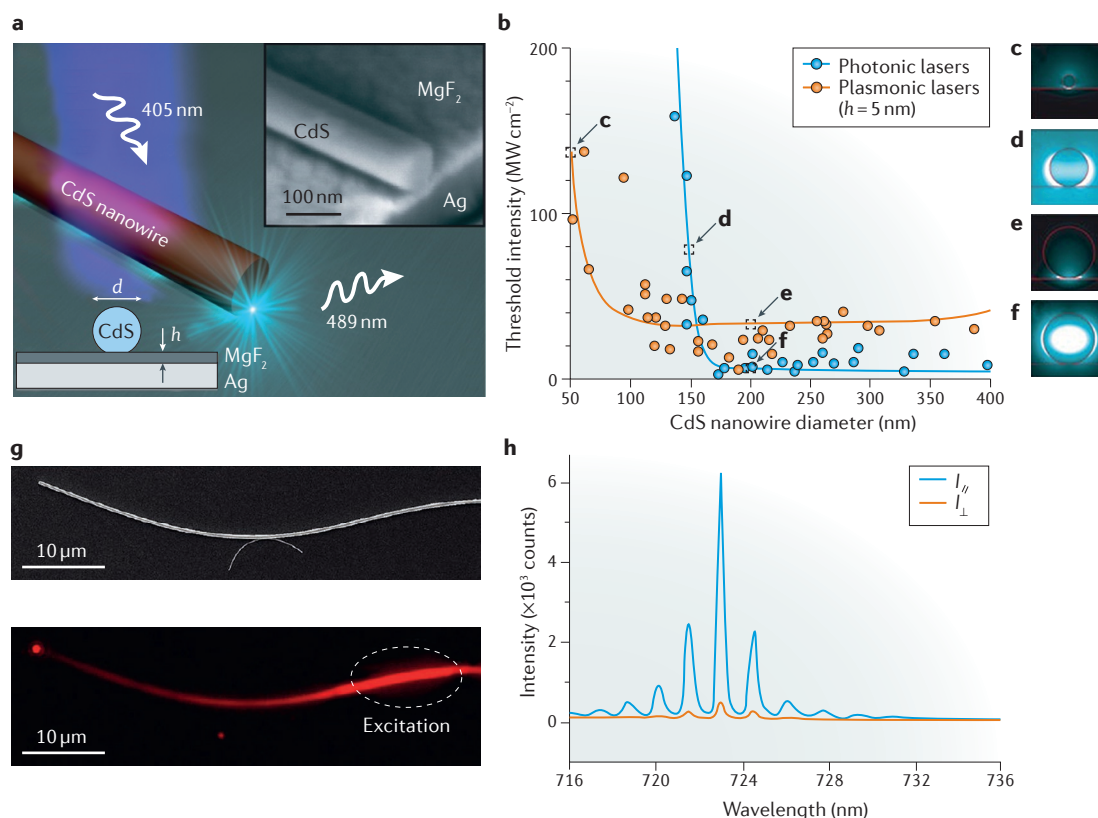


Figure 6 | Surface plasmon polaritons lead to further laser miniaturization. **a** | Depiction of a CdS nanowire on a silver substrate forming a SPP laser cavity under optical excitation. **b** | Lasing threshold intensity as a function of nanowire diameter for photonic and plasmonic laser cavities. SPP nanowire cavities are able to lase with significantly smaller diameters than photonic cavities indicating the plasmonic nature of the cavity. **c–f** | Simulations of guided modes for plasmonic (panels **c** and **d**) and photonic (panels **e** and **f**) nanowire laser cavities. **g** | Scanning electron micrograph (top) and optical image (bottom) of a CdSe nanowire coupled to a silver nanowire. **h** | Excitation of the CdSe nanowire results in polarization-dependent emission from the silver nanowire end facet. *d*, diameter; *h*, height; I_{\parallel} , emission intensity with parallel polarization; I_{\perp} , emission intensity with perpendicular polarization; SPP, surface plasmon polariton. Panels **a–f** are from REF. 96, Nature Publishing Group. Panels **g** and **h** are adapted with permission from REF. 99, American Chemical Society.

cavity has been improved substantially over the years, but mechanical instability has been a significant issue that has limited the application of these cavities. In a recent report, the mechanical stability of the ring resonator was improved by splicing the ends together using a short polystyrene nanowire segment⁸³. Although the splice increased the lasing threshold slightly, the enhanced mechanical stability should allow for a wider range of applications, including their use in liquid media.

Alternative cavity geometries have also been explored to improve nanowire laser performance. Single-mode lasing is highly desirable for applications in sensing, optical communications, spectroscopy and interferometry. The simplest way to achieve single-mode lasing in nanowires is by reducing the length to expand the free spectral range, such that only one longitudinal mode exists in the luminescence bandwidth⁸⁴. However, this results in an increased lasing threshold, because the shorter cavity length reduces the round-trip gain. One alternative strategy relies on the formation of a cleaved-coupled cavity²⁶. By cleaving a nanowire at a determined point, all but a single lasing mode may be suppressed by modulating the loss at the air gap. Successful device fabrication relies

on calculations of both the gap position and the size of each cavity to modulate the lasing threshold of all the longitudinal modes. This process was recently shown for a GaN nanowire that was cleaved using focused ion-beam milling (FIG. 5). This study demonstrated that the emission quality can be improved by increasing the gain in a single nanowire in a specified geometry, which reduces the lasing threshold. Another strategy to achieve single-mode lasing relies on the use of 'loop mirrors', in which the nanowire is bent into a loop, resulting in both high effective reflectivity and a shortened cavity path length⁸⁵. By bending a CdSe nanowire to include zero, one or two loop mirrors, a threefold decrease in the lasing threshold and near single-mode lasing were observed. As the nanowire properties are dependent on the size and geometry of the laser mirrors, both the lasing threshold and modes may be tuned.

The assembly of nanowires into hierarchical photonic structures and their integration into microresonator structures to form hybrid photonic devices are also of great interest for exploring cutting-edge optical phenomena. These devices rely on supporting structures that are optically coupled to a nanowire that provides gain. The

first study involved coupling a CdS nanowire to a resonator microcavity⁸⁶. The microcavity design was guided by finite-difference time-domain simulations to demonstrate that lasing was possible in either linear or race-track-style microcavities. An alternative process used a bottom-up synthesis exclusively to grow a photonic crystal composed of a well-ordered nanowire array⁸⁷. Each nanowire was made up of a GaAs–InGaAs–GaAs axial heterostructure, with the central InGaAs section acting as the gain medium. These advances in incorporating nanowires into hierarchical or other photonic structures showcase the flexibility of nanowires for integration with photonic structures. Taking these integration concepts a step further, a GaN nanowire was used to reduce the threshold of a room-temperature polariton laser⁸⁸. This feat was accomplished by integrating a GaN nanowire grown inside a microcavity with the nanowire growth direction perpendicular to the optical axis of the cavity. This strategy avoided the internal polarization field of GaN, which probably reduced the quantum efficiency in previously reported GaN-based microcavity lasers via the quantum-confined Stark effect⁸⁹. These studies highlight how nanowires can be used with conventional photonic structures to explore optical phenomena, and they also emphasize the excellent optical performance of nanowire-based devices.

Surface plasmon polariton lasers

The miniaturization of semiconductor nanowire lasers is limited by the diffraction limit, which is approximately half of the optical wavelength in the medium. In general, reducing the diameter of the nanowire leads to poor optical confinement and small modal gain, which make photonic lasing impossible. However, nanowires can be used as platforms for creating a new type of laser based on surface plasmon polaritons (SPPs)^{90,91}. SPP waves, which are the collective oscillations of electrons on the surface of a metal, have significantly shorter wavelengths than photonic wavelengths of the same energy, which allows the laser cavity to store and guide optical energy far below the optical diffraction limit. The main challenge in creating a plasmonic laser has been to overcome the intrinsic absorption loss of the metal⁹², which prevents optical energy from amplifying in a cavity. The strategy of applying a silver coating to a nanowire laser to harness SPPs for lasing and to reduce the overall size of the laser structure was first studied theoretically⁹³ in 2007. This study suggested the existence of wavelength regions in which the nanowire optical gain could exceed the metal loss — the process of optical energy absorption and dissipation via electron scattering and thermalization in a metal — to achieve an overall positive gain. To further minimize this loss, a new type of cavity was created by placing a dielectric spacer between the metal and the gain medium to create a hybrid plasmonic cavity^{94,95}. This strategy allows most of the optical energy to be contained in the spacer rather than in the metal, thereby reducing metal loss.

Early theoretical work predicted that a dielectric–metal hybrid structure could be a successful platform for lasing⁹⁵. This was followed by the first report of SPP nanowire lasing in a horizontal CdS nanowire on a silver

substrate, separated by a nanoscale film of MgF₂ that provides control over optical confinement, insulates the wire from the metal and provides a transverse hybrid cavity⁹⁶ (FIG. 6). Through optical pumping, characteristic signatures of lasing were observed that indicated that the plasmonic nanowires were operating in a Fabry–Pérot geometry. Photonic lasing was also easily achieved by exchanging the silver substrate with quartz, which allowed for a direct performance comparison. Although both types of lasing exhibited similar thresholds owing to their similar cavity structures, there was a significant difference in their diameter dependences. With decreasing nanowire diameter, photonic lasing ceased near 150 nm as optical confinement broke down, whereas plasmonic lasing persisted down to 52 nm. Furthermore, measurements of the emission polarization confirmed the existence of plasmonic modes, because plasmons are strictly longitudinal, whereas photonic modes have significant transverse polarization. In addition, similar research based on GaN nanowires on single-crystal silver⁹⁷ and ZnO nanowires⁹⁸ for operation near the SPP resonance has continued in the past few years, leading to interesting new results for low-threshold⁹⁷ and ultrafast⁹⁸ operation.

One of the drawbacks of a transverse hybrid cavity is the inability to separate contributions from the plasmonic and photonic components. A unique cavity scheme was devised to address this issue: a curved CdSe nanowire was coupled to a small point at the side of a curved silver nanowire⁹⁹. This arrangement produced a longitudinal hybrid cavity, in which optical excitation of the CdSe nanowire and subsequent waveguiding generated SPP waves in the silver nanowire. Moreover, the geometry provided spatial separation between simultaneous plasmonic and photonic contributions to the emission output. Upon excitation of the CdSe portion of the cavity, light output was observed from the silver nanowire end of the cavity, indicating efficient photon-to-plasmon coupling. By measuring the emission output from the silver nanowire, a strong polarization dependence was observed, indicative of the electromagnetic nature of the SPP waves. An interesting feature of this demonstration is that a strongly localized, coherent, SPP source could be ‘delivered’ to another point. Although great challenges still exist in minimizing metal loss and improving the overall gain efficiency, SPP nanowire lasers offer significant advantages, such as improved thermal management.

Electrical excitation of nanowire lasers

The nanowire lasers discussed thus far are excited optically by another laser that is orders of magnitude larger. Although this is suitable for the fundamental study and development of new gain media and cavity architectures, optical excitation is unsuitable for most of the intended nanowire laser applications, especially in the area of on-chip integrated photonics. Therefore, carrier excitation via electrical pumping is a much more desirable approach. The ultimate goal for semiconductor nanowire lasing hinges on achieving reliable lasing through the electrical injection of electrons and holes into a dielectric–metal composite nanowire structure. The principal challenge in realizing electrically pumped nanowire

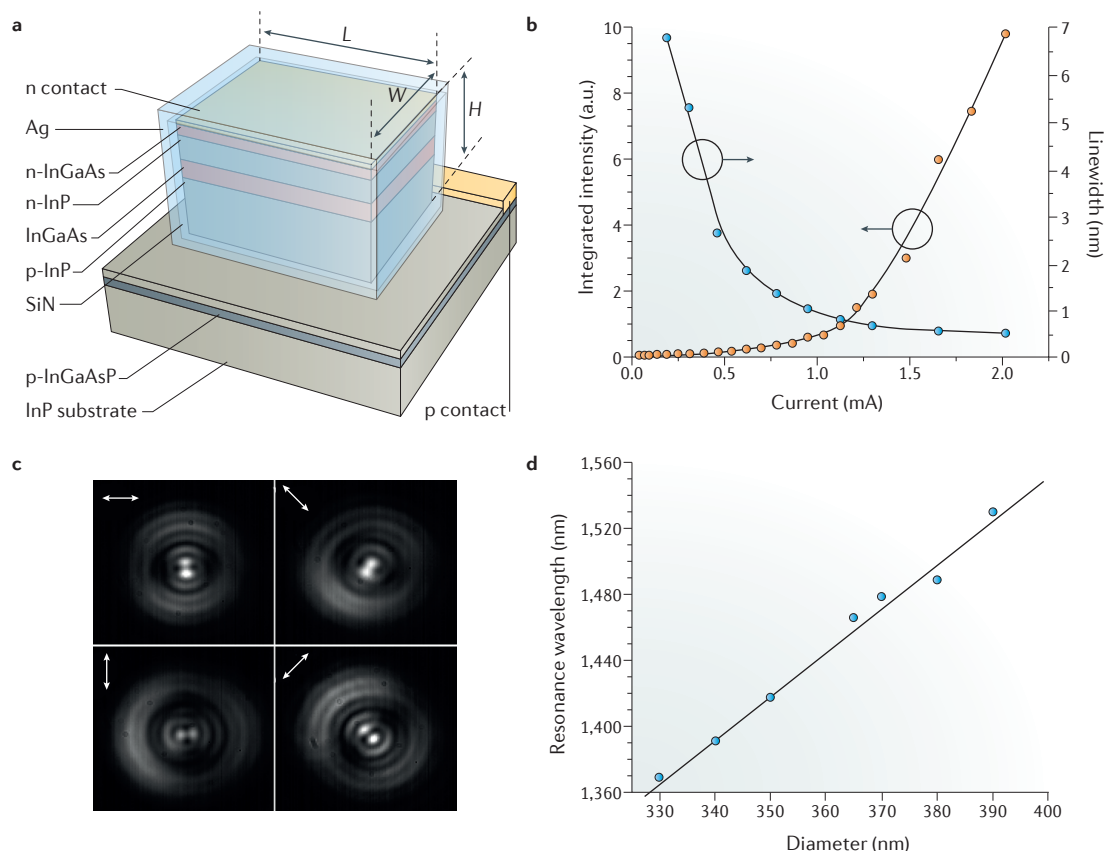


Figure 7 | Fabrication and characterization of electrically pumped nanowire lasers. **a** | Cross-sectional diagram of an InGaAs–InP metallic laser cavity. **b** | Integrated emission intensity (orange) and linewidth (blue) as a function of device current showing a superlinear increase of emission with decreasing linewidth. **c** | Four polarized emission images (polarizer direction is given by the white arrows) from a cylindrical, electrically pumped cavity demonstrating azimuthal emission polarization. **d** | The linear dependence between the nanowire cavity diameter and laser emission wavelength. a.u., arbitrary units. Panels **a** and **b** are adapted with permission from REF. 104, The Optical Society. Panels **c** and **d** are adapted with permission from REF. 105, copyright 2013, AIP Publishing LLC.

lasers is to integrate electrodes without diminishing the quality of the cavity to the point that lasing is no longer possible. Similar to plasmonic lasers, metal loss has been identified as the primary loss mechanism in electrically pumped cavities⁹². Overcoming this has been a high priority and has been pursued through several different approaches.

Lithographic, top-down techniques are currently the most viable approach for producing electrically driven nanowire lasers. In the first report of electrically pumped nanowire lasing, a horizontal CdS nanowire on a Si (p^{2+}) substrate was coated with an insulating layer of Al_2O_3 followed by a Ti–Au injection layer¹⁰⁰. Almost a decade passed before another promising device architecture arose — the semiconductor core–metal shell⁹³ structure, which was realized using a top-down fabrication process¹⁰¹. Extensive modelling and experimental work demonstrated that a semiconductor–metal core–shell structure can facilitate gain for lasing and is amenable for electrical injection^{93,101,102}. As a demonstration of electrical injection lasing, an n–InP/InGaAs/p–InP micropillar was etched from a metalorganic chemical vapour deposition-grown wafer to provide the gain medium and optical cavity, while current injection was provided

by a p–InGaAsP substrate and a Ag–SiN conductor–insulator layer¹⁰³ (FIG. 7). The initial devices demonstrated light emission that was characteristic of lasing, but their performance was inhibited by significant heating. This barrier was recently overcome by improving the structure and thermal management of the device^{102,104}. The newest generation of devices shows lasing thresholds of 1.2 mA under DC bias and operation at more than twice the threshold current. This remarkable work is the first well-understood demonstration of lasing in a near-nanosized cavity. A subsequent study built on this by showing that control over the lasing wavelength as well as emission polarization was possible¹⁰⁵. A similar, cylindrical cavity was electrically pumped and found to output azimuthally polarized light, which is crucial for particle trapping and high-resolution imaging. Facile lasing wavelength control from 1.37 to 1.53 μ m was achieved by adjusting the cavity diameter during device fabrication.

Another strategy for electrical pumping relies on nanowire arrays grown directly on conducting substrates followed by post-synthetic introduction of the second contact. Electrically pumped random lasing in AlGaIn nanowire arrays has recently been reported¹⁰⁶. By using

the Anderson localization of light in AlGaIn–GaIn heterostructures, random lasing in the UV spectral region was achieved in a lithography-free nanowire array. The nanowire array was grown using molecular beam epitaxy to form an AlGaIn active layer sandwiched between two p- and n-doped AlGaIn cladding layers, with the structures templated from Si-doped GaIn on n-Si. Successful continuous-wave operation was observed from 6 to 100 K, with a lasing threshold of 12 A cm^{-2} and an operational stability at over 6 times the threshold current. Emission wavelength tunability from 319 to 335 nm was also observed for various regions depending on the nature of the gain cavity. Further wavelength tunability was achieved afterwards by using quantum confinement¹⁰⁷. The AlGaIn gain medium was fabricated as a collection of nanoparticles that lased at 262.1 nm with comparable lasing thresholds at 77 K. These reports show some potentially promising directions for developing better electrically injected nanowire lasers.

Conclusions and outlook

Research conducted over the past fifteen years has significantly advanced the field of semiconductor nanowire lasers. In particular, great progress has been made by expanding the range of available materials and cavity structures, achieving greater control over the alloy composition and lasing mode, and reducing lasing thresholds. Wavelength-tunable, solution-processable perovskite nanowire lasers are a promising class of materials capable of record-breaking performance. Improvement of the design, performance and overall understanding of plasmonic nanowire lasers opens up promising avenues for the development of ultrascale laser cavities. Although important advances have been made, such as achieving room temperature operation, which was initially thought to be impossible, new designs and a reduction of metal loss are still crucial for further improving device performance. Finally, with more progress in the development of electrically pumped nanoscale lasers, future integration of these devices into optoelectronic circuits is within reach. Ultimately, semiconductor nanowire lasers are incredibly versatile nanoscale light sources. Although they vary widely in terms of their composition, geometry, cavity structure and lasing mechanism, they all have the potential to supply light for integrated photonics applications. By expanding the

capabilities and improving the performance of semiconductor nanowire lasers, the scientific community will surely discover new insights and applications.

Although great progress has been made in exploring the semiconductor nanowire laser design space, difficult challenges remain on many fronts. First, it is of utmost importance that nanowire lasers that can operate under electrical injection can be produced routinely and reproducibly, especially on the level of individual nanowires. Electrical injection is almost a necessity for all semiconductor laser applications, especially for integrated photonics. To achieve this, improved injection geometry is needed, as well as the fabrication of small, low-resistance contacts that do not significantly perturb the optical cavity. In addition, control of the nanowire doping profile has been demonstrated, but reproducibility must be improved. Nanowire array lasers under electrical injection also provide an interesting route forward. Although such lasers are not necessarily small compared with individual nanowire lasers, these approaches offer important alternatives to traditional laser fabrication in terms of material growth on lattice-mismatched substrates, as well as allowing access to wavelength ranges that are not otherwise accessible.

Second, further systematic study is needed at the device level to investigate the absolute power efficiency, lifetime, reliability and reproducibility of nanowire laser devices. This will allow for comprehensive improvements to make nanowire lasers more ‘application ready’. These studies are a necessary next step after fifteen years of materials research and development of proof-of-concept devices.

Third, although preliminary demonstrations of the applications of nanowires and nanowire lasers have shown great potential in a wide range of areas, these demonstrations need to be extended, both in depth and breadth. Nanowire-based multicolour and white lasers offer unique possibilities that are not available in traditional, planar materials. The application of multicolour lasers in displays and lighting should be more seriously and systematically pursued. The integration of different components on a single platform is a great advantage of nanowire-based technology and has only been demonstrated sporadically to date. Such integration could open a wide range of applications beyond information technology, such as in nanofluidics-based biological and chemical detection and sensing.

- Einstein, A. Strahlungs-Emission und Absorption nach der Quantentheorie. *Dtsch. Phys. Ges.* **18**, 318–323 (1916).
- Schawlow, A. L. & Townes, C. H. Infrared and optical masers. *Phys. Rev.* **112**, 1940–1949 (1958).
- Maiman, T. H. Stimulated optical radiation in ruby. *Nature* **187**, 493–494 (1960).
- Council, N. R. in *Optics and Photonics: Essential Technologies for our Nation* 20–63 (The National Academies Press, 2013).
- Agrawal, G. P. & Dutta, N. K. in *Semiconductor Lasers* 547–582 (Springer, 1993).
- Choquette, K. D. & Hou, H. Q. Vertical-cavity surface emitting lasers: moving from research to manufacturing. *Proc. IEEE* **85**, 1730–1739 (1997).
- Mahler, L. *et al.* Vertically emitting microdisk lasers. *Nat. Photonics* **3**, 46–49 (2009).
- Altug, H. & Vučković, J. Photonic crystal nanocavity array laser. *Opt. Express* **13**, 8819–8828 (2005).
- Ning, C. Z. in *Advances in Semiconductor Lasers* (eds Coleman, J. J., Bryce, A. C. & Jagadish, C.) 455–486 (Academic Press, 2012).
- Ma, R.-M., Ota, S., Li, Y., Yang, S. & Zhang, X. Explosives detection in a lasing plasmon nanocavity. *Nat. Nanotechnol.* **9**, 600–604 (2014).
- Ma, Y., Guo, X., Wu, X., Dai, L. & Tong, L. Semiconductor nanowire lasers. *Adv. Opt. Photonics* **5**, 216–273 (2013).
- Yan, R., Gargas, D. & Yang, P. Nanowire photonics. *Nat. Photonics* **3**, 569–576 (2009).
- Wagner, R. S. & Ellis, W. C. Vapor–liquid–solid mechanism of single crystal growth. *Appl. Phys. Lett.* **4**, 89–90 (1964).
- Huang, M. H. *et al.* Room-temperature ultraviolet nanowire nanolasers. *Science* **292**, 1897–1899 (2001).
- Huang, M. H. *et al.* Catalytic growth of zinc oxide nanowires by vapor transport. *Adv. Mater.* **13**, 113–116 (2001).
- Johnson, J. C. *et al.* Single gallium nitride nanowire lasers. *Nat. Mater.* **1**, 106–110 (2002).
- Johnson, J. C. *et al.* Single nanowire lasers. *J. Phys. Chem. B* **105**, 11387–11390 (2001).
- Zimmler, M. A., Capasso, F., Müller, S. & Ronning, C. Optically pumped nanowire lasers: invited review. *Semicond. Sci. Technol.* **25**, 024001 (2010).
- Maslov, A. V. & Ning, C. Z. Far-field emission of a semiconductor nanowire laser. *Opt. Lett.* **29**, 572–574 (2004).
- Coldren, L. A. & Corzine, S. W. in *Diode Lasers and Photonic Integrated Circuits* 247–334 (Wiley, 1995).
- Siegman, A. E. in *Lasers* 457–557 (Univ. Science Books, 1986).
- Maslov, A. V. & Ning, C. Z. Reflection of guided modes in a semiconductor nanowire laser. *Appl. Phys. Lett.* **83**, 1237–1239 (2003).

23. Maslov, A. V. & Ning, C. Z. Modal gain in a semiconductor nanowire laser with anisotropic bandstructure. *IEEE J. Quant. Electron.* **40**, 1389–1397 (2004).
24. Ning, C. Z. *et al.* in *Photonics Society Summer Topical Meeting Series, IEEE 23–24* (Montréal, 2014).
25. Ning, C. Z. What is laser threshold. *IEEE J. Sel. Top. Quantum Electron.* **19**, 1503604 (2013).
26. Gao, H., Fu, A., Andrews, S. C. & Yang, P. Cleaved-coupled nanowire lasers. *Proc. Natl Acad. Sci. USA* **110**, 865–869 (2013).
27. Chow, W. W., Jahnke, F. & Gies, C. Emission properties of nanolasers during the transition to lasing. *Light Sci. Appl.* **3**, e201 (2014).
28. Björk, G., Karlsson, A. & Yamamoto, Y. Definition of a laser threshold. *Phys. Rev. A* **50**, 1675–1680 (1994).
29. Zimmer, M. A., Bao, J., Capasso, F., Müller, S. & Rønning, C. Laser action in nanowires: observation of the transition from amplified spontaneous emission to laser oscillation. *Appl. Phys. Lett.* **93**, 051101 (2008).
30. Johnson, J. C., Yan, H., Yang, P. & Saykally, R. J. Optical cavity effects in ZnO nanowire lasers and waveguides. *J. Phys. Chem. B* **107**, 8816–8828 (2003).
31. Choi, H.-J. *et al.* Self-organized GaN quantum wire UV lasers. *J. Phys. Chem. B* **107**, 8721–8725 (2003).
32. Seo, M.-K. *et al.* Modal characteristics in a single-nanowire cavity with a triangular cross section. *Nano Lett.* **8**, 4534–4538 (2008).
33. Gradečak, S., Qian, F., Li, Y., Park, H.-G. & Lieber, C. M. GaN nanowire lasers with low lasing thresholds. *Appl. Phys. Lett.* **87**, 173111 (2005).
34. Qian, F. *et al.* Multi-quantum-well nanowire heterostructures for wavelength-controlled lasers. *Nat. Mater.* **7**, 701–706 (2008).
35. Agarwal, R., Barrelet, C. J. & Lieber, C. M. Lasing in single cadmium sulfide nanowire optical cavities. *Nano Lett.* **5**, 917–920 (2005).
36. Pan, A. *et al.* Fabrication and red-color lasing of individual highly uniform single-crystal CdSe nanobelts. *J. Phys. Chem. C* **111**, 14253–14256 (2007).
37. Pan, A. *et al.* Continuous alloy-composition spatial grading and superbroad wavelength-tunable nanowire lasers on a single chip. *Nano Lett.* **9**, 784–788 (2009).
38. Saxena, D. *et al.* Optically pumped room-temperature GaAs nanowire lasers. *Nat. Photonics* **7**, 963–968 (2013).
39. Chen, R. *et al.* Nanolasers grown on silicon. *Nat. Photonics* **5**, 170–175 (2011).
40. Mayer, B. *et al.* Lasing from individual GaAs–AlGaAs core–shell nanowires up to room temperature. *Nat. Commun.* **4**, 2931 (2013).
41. Zapfen, J. A. *et al.* Room-temperature single nanoribbon lasers. *Appl. Phys. Lett.* **84**, 1189–1191 (2004).
42. Chin, A. H. *et al.* Near-infrared semiconductor subwavelength-wire lasers. *Appl. Phys. Lett.* **88**, 163115 (2006).
43. Gao, Q. *et al.* Selective-area epitaxy of pure wurtzite InP nanowires: high quantum efficiency and room-temperature lasing. *Nano Lett.* **14**, 5206–5211 (2014).
44. Zhang, L. *et al.* Wide InP nanowires with wurtzite/zincblende superlattice segments are type II whereas narrower nanowires become type I: an atomistic pseudopotential calculation. *Nano Lett.* **10**, 4055–4060 (2010).
45. Kotani, A. *et al.* Endov/DNA ligase mutation scanning assay using microchip capillary electrophoresis and dual-color laser-induced fluorescence detection. *Anal. Methods* **4**, 58–64 (2012).
46. Neumann, A. *et al.* Four-color laser white illuminant demonstrating high color-rendering quality. *Opt. Express* **19**, A982–A990 (2011).
47. Fan, F., Turkdogan, S., Liu, Z., Shelhammer, D. & Ning, C. Z. A monolithic white laser. *Nat. Nanotechnol.* **10**, 796–803 (2015).
48. Li, J. *et al.* Wavelength tunable CdSe nanowire lasers based on the absorption-emission-absorption process. *Adv. Mater.* **25**, 833–837 (2013).
49. Liu, X., Zhang, Q., Yip, J. N., Xiong, Q. & Sum, T. C. Wavelength tunable single nanowire lasers based on surface plasmon polariton enhanced Burstein–Moss effect. *Nano Lett.* **13**, 5336–5343 (2013).
50. Pauzauskie, P. J., Sirbuldy, D. J. & Yang, P. Semiconductor nanowire ring resonator laser. *Phys. Rev. Lett.* **96**, 143903 (2006).
51. Xiao, Y., Meng, C., Wu, X. & Tong, L. Single mode lasing in coupled nanowires. *Appl. Phys. Lett.* **99**, 023109 (2011).
52. Zhuang, X., Ning, C. Z. & Pan, A. Composition and bandgap-graded semiconductor alloy nanowires. *Adv. Mater.* **24**, 13–33 (2012).
53. Zapfen, J. A. *et al.* Continuous near-infrared-to-ultraviolet lasing from II–VI nanoribbons. *Appl. Phys. Lett.* **90**, 213114 (2007).
54. Kuykendall, T., Ulrich, P., Aloni, S. & Yang, P. Complete composition tunability of InGaN nanowires using a combinatorial approach. *Nat. Mater.* **6**, 951–956 (2007).
55. Pan, A., Liu, R., Sun, M. & Ning, C.-Z. Quaternary alloy semiconductor nanobelts with bandgap spanning the entire visible spectrum. *J. Am. Chem. Soc.* **131**, 9502–9503 (2009).
56. Pan, A., Liu, R., Sun, M. & Ning, C.-Z. Spatial composition grading of quaternary ZnCdSse alloy nanowires with tunable light emission between 350 and 710 nm on a single substrate. *ACS Nano* **4**, 671–680 (2010).
57. Gu, F. *et al.* Spatial bandgap engineering along single alloy nanowires. *J. Am. Chem. Soc.* **133**, 2037–2039 (2011).
58. Xu, J. *et al.* Asymmetric light propagation in composition-graded semiconductor nanowires. *Sci. Rep.* **2**, 820 (2012).
59. Liu, Z. *et al.* Dynamical color-controllable lasing with extremely wide tuning range from red to green in a single alloy nanowire using nanoscale manipulation. *Nano Lett.* **13**, 4945–4950 (2013).
60. Yang, Z. *et al.* Broadly defining lasing wavelengths in single bandgap-graded semiconductor nanowires. *Nano Lett.* **14**, 3153–3159 (2014).
61. Green, M. A., Ho-Baillie, A. & Snaith, H. J. The emergence of perovskite solar cells. *Nat. Photonics* **8**, 506–514 (2014).
62. Snaith, H. J. Perovskites: the emergence of a new era for low-cost, high-efficiency solar cells. *J. Phys. Chem. Lett.* **4**, 3623–3630 (2013).
63. Xing, G. *et al.* Low-temperature solution-processed wavelength-tunable perovskites for lasing. *Nat. Mater.* **13**, 476–480 (2014).
64. Deschler, F. *et al.* High photoluminescence efficiency and optically pumped lasing in solution-processed mixed halide perovskite semiconductors. *J. Phys. Chem. Lett.* **5**, 1421–1426 (2014).
65. Stranks, S. D. *et al.* Enhanced amplified spontaneous emission in perovskites using a flexible cholesteric liquid crystal reflector. *Nano Lett.* **15**, 4935–4941 (2015).
66. Zhu, H. *et al.* Lead halide perovskite nanowire lasers with low lasing thresholds and high quality factors. *Nat. Mater.* **14**, 636–642 (2015).
67. Xing, J. *et al.* Vapor phase synthesis of organometal halide perovskite nanowires for tunable room-temperature nanolasers. *Nano Lett.* **15**, 4571–4577 (2015).
68. Niu, G., Guo, X. & Wang, L. Review of recent progress in chemical stability of perovskite solar cells. *J. Mater. Chem. A* **3**, 8970–8980 (2015).
69. Conings, B. *et al.* Intrinsic thermal instability of methylammonium lead trihalide perovskite. *Adv. Energy Mater.* **5**, 1500477 (2015).
70. Fu, Y. *et al.* Nanowire lasers of formamidinium lead halide perovskites and their stabilized alloys with improved stability. *Nano Lett.* **16**, 1000–1008 (2016).
71. Lee, J.-W. *et al.* Formamidinium and cesium hybridization for photo- and moisture-stable perovskite solar cell. *Adv. Energy Mater.* **5**, 1501310 (2015).
72. Nedelcu, G. *et al.* Fast anion-exchange in highly luminescent nanocrystals of cesium lead halide perovskites (CsPbX₃, X = Cl, Br, I). *Nano Lett.* **15**, 5635–5640 (2015).
73. Protesescu, L. *et al.* Nanocrystals of cesium lead halide perovskites (CsPbX₃, X = Cl, Br, and I): novel optoelectronic materials showing bright emission with wide color gamut. *Nano Lett.* **15**, 3692–3696 (2015).
74. Wang, Y. *et al.* All-inorganic colloidal perovskite quantum dots: a new class of lasing materials with favorable characteristics. *Adv. Mater.* **27**, 7101–7108 (2015).
75. Yakunin, S. *et al.* Low-threshold amplified spontaneous emission and lasing from colloidal nanocrystals of cesium lead halide perovskites. *Nat. Commun.* **6**, 8056 (2015).
76. Zhang, D., Eaton, S. W., Yu, Y., Dou, L. & Yang, P. Solution-phase synthesis of cesium lead halide perovskite nanowires. *J. Am. Chem. Soc.* **137**, 9230–9233 (2015).
77. Eaton, S. W. *et al.* Lasing in robust cesium lead halide perovskite nanowires. *Proc. Natl Acad. Sci. USA* **113**, 1993–1998 (2016).
78. Sirbuldy, D. J. *et al.* Optical routing and sensing with nanowire assemblies. *Proc. Natl Acad. Sci. USA* **102**, 7800–7805 (2005).
79. Greytak, A. B., Barrelet, C. J., Li, Y. & Lieber, C. M. Semiconductor nanowire laser and nanowire waveguide electro-optic modulators. *Appl. Phys. Lett.* **87**, 151103 (2005).
80. Shambat, G. *et al.* Single-cell photonic nanocavity probes. *Nano Lett.* **13**, 4999–5005 (2013).
81. Yang, P. *et al.* Controlled growth of ZnO nanowires and their optical properties. *Adv. Funct. Mater.* **12**, 323–331 (2002).
82. Yan, H. *et al.* Dendritic nanowire ultraviolet laser array. *J. Am. Chem. Soc.* **125**, 4728–4729 (2003).
83. Hu, Z., Guo, X. & Tong, L. Freestanding nanowire ring laser. *Appl. Phys. Lett.* **103**, 183104 (2013).
84. Li, O. *et al.* Single-mode GaN nanowire lasers. *Opt. Express* **20**, 17873–17879 (2012).
85. Xiao, Y. *et al.* Single-nanowire single-mode laser. *Nano Lett.* **11**, 1122–1126 (2011).
86. Barrelet, C. J. *et al.* Hybrid single-nanowire photonic crystal and microresonator structures. *Nano Lett.* **6**, 11–15 (2006).
87. Scofield, A. C. *et al.* Bottom-up photonic crystal lasers. *Nano Lett.* **11**, 5387–5390 (2011).
88. Das, A. *et al.* Room temperature ultralow threshold GaN nanowire polariton laser. *Phys. Rev. Lett.* **107**, 066405 (2011).
89. Hisashi, M. *et al.* Quantum-confined stark effect on photoluminescence and electroluminescence characteristics of InGaN-based light-emitting diodes. *J. Phys. D: Appl. Phys.* **41**, 165105 (2008).
90. Zhang, T. & Shan, F. Development and application of surface plasmon polaritons on optical amplification. *J. Nanomater.* **2014**, 495381 (2014).
91. Berini, P. & De Leon, I. Surface plasmon–polariton amplifiers and lasers. *Nat. Photonics* **6**, 16–24 (2012).
92. Khurgin, J. B. How to deal with the loss in plasmonics and metamaterials. *Nat. Nanotechnol.* **10**, 2–6 (2015).
93. Maslov, A. V. & Ning, C. Z. Size reduction of a semiconductor nanowire laser by using metal coating. *Proc. SPIE* **6468**, 64680I (2007).
94. Oulton, R. F. Surface plasmon lasers: sources of nanoscopic light. *Mater. Today* **15**, 26–34 (2012).
95. Oulton, R. F., Sorger, V. J., Genov, D. A., Pile, D. F. P. & Zhang, X. A hybrid plasmonic waveguide for subwavelength confinement and long-range propagation. *Nat. Photonics* **2**, 496–500 (2008).
96. Oulton, R. F. *et al.* Plasmon lasers at deep subwavelength scale. *Nature* **461**, 629–632 (2009).
97. Lu, Y.-J. *et al.* Plasmonic nanolaser using epitaxially grown silver film. *Science* **337**, 450–453 (2012).
98. Sidiropoulos, T. P. H. *et al.* Ultrafast plasmonic nanowire lasers near the surface plasmon frequency. *Nat. Phys.* **10**, 870–876 (2014).
99. Wu, X. *et al.* Hybrid photon–plasmon nanowire lasers. *Nano Lett.* **13**, 5654–5659 (2013).
100. Duan, X., Huang, Y., Agarwal, R. & Lieber, C. M. Single-nanowire electrically driven lasers. *Nature* **421**, 241–245 (2003).
101. Hill, M. T. *et al.* Lasing in metallic-coated nanocavities. *Nat. Photonics* **1**, 589–594 (2007).
102. Ding, K. & Ning, C. Z. Fabrication challenges of electrical injection metallic cavity semiconductor nanolasers. *Semicond. Sci. Technol.* **28**, 124002 (2013).
103. Ding, K. *et al.* Room-temperature continuous wave lasing in deep-subwavelength metallic cavities under electrical injection. *Phys. Rev. B: Condens. Matter* **85**, 041301 (2012).
104. Ding, K. *et al.* Record performance of electrical injection sub-wavelength metallic-cavity semiconductor lasers at room temperature. *Opt. Express* **21**, 4728–4733 (2013).
105. Ding, K. *et al.* An electrical injection metallic cavity nanolaser with azimuthal polarization. *Appl. Phys. Lett.* **102**, 041110 (2013).
106. Li, K. H., Liu, X., Wang, Q., Zhao, S. & Mi, Z. Ultralow-threshold electrically injected AlGaIn nanowire ultraviolet lasers on Si operating at low temperature. *Nat. Nanotechnol.* **10**, 140–144 (2015).
107. Zhao, S. *et al.* An electrically injected AlGaIn nanowire laser operating in the ultraviolet-C band. *Appl. Phys. Lett.* **107**, 043101 (2015).

Acknowledgements

Work performed at the University of California, Berkeley was supported by the U.S. Department of Energy under contract no. DE-AC02-05CH11231 (PChem KC3103). Work performed at Arizona State University was supported by DARPA (W911NF-07-1-0314), AFOSR (Grant No FA9550-10-1-0444 under Gernot Pomrenke), and ARO (award no. W911NF-08-1-0471 and W911NF-13-1-0278, under M. Gerhold) and at Tsinghua University by the National 985 University Project. S.W.E. thanks the Camille and Henry Dreyfus Foundation for funding (Award EP-14-151).

Competing interests statement

The authors declare no competing interests.